Enhanced self-training superresolution mapping technique for hyperspectral imagery

Journal:	*Geoscience and Remote Sensing Letters*
Manuscript ID:	GRSL-00345-2010.R3
Manuscript Type:	Letters
Date Submitted by the Author:	n/a
Complete List of Authors:	A. Mianji, Fereidoun; Harbin Institute of Technology, School of Electronics and Information Technology Zhang, Ye; Harbin Institute of Technology, School of Electronics and Information Technology Gu, Yanfeng; Harbin Institute of Technology, School of Electronics and Information Technology Zhang, Junping; Harbin Institute of Technology, School of Electronics and Information Technology
Key Words:	Image processing, Image analysis, Image enhancement

Enhanced Self-Training Superresolution Mapping Technique for Hyperspectral Imagery

Fereidoun A. Mianji, *Student Member, IEEE*, Ye Zhang, *Member, IEEE*, Yanfeng Gu, *Member, IEEE*, and Junping Zhang, *Member, IEEE*

***Abstract*-**An efficient superresolution technique through spatial-spectral data fusion for hyperspectral (HS) imagery is proposed in this paper. The spatial and spectral contents of a HS image are extracted using a linear mixture model and a fully constrained least squares unmixing technique. These data are then combined using a spatial correlation model through a learning-based superresolution mapping (SRM) algorithm. The proposed spatial correlation model realistically simulates a mapping model between the low resolution (LR) HS image and its subsampled version (LR^2 HS image) to train the designed SRM algorithm for mapping from the LR to HR (high resolution). The experiments on real HS images validate the accuracy and low complexity of the proposed autonomous technique for key information detection in hyperspectral imagery.

***Index Terms*-**Data fusion, hyperspectral imagery, key information detection, linear mixture model, superresolution mapping.

I. INTRODUCTION

A significant problem in hyperspectral (HS) remote sensing concerns the sensor spatial resolution. This restricts the size of an object able to be detected on the ground. In a number of proposed enhancing methods a high resolution (HR) image is needed to improve the low resolution (LR) HS image [1]. Spectral mixture analysis (SMA) or subpixel classification is another well-known approach which often provides a more accurate representation of landcovers compared to the original HS image [2]. Although, SMA does not need any supplementary source of information, it only describes mixed pixels by the abundances of endmembers without defining the spatial distribution of the endmembers within the pixels. Another group of effective but complex investigated techniques is based on superresolution mapping (SRM). SRM exploits the spatial-spectral information of HS images using a high resolution (HR) image or a model [2]-[6]. Despite the success of these approaches, they suffer at least one of the aforementioned shortcomings. In this paper we propose a novel fast and efficient image enhancement technique to tackle these limitations.

The proposed method realistically adopts a learning-based SRM algorithm to extrapolate the simulated LR^2 (subsampled LR) to LR mapping model of an HS image to a successful LR to HR mapping. This method is referred to as self-training technique since it uses the input data as the source of training samples in an unsupervised fashion and is independent of any secondary HR image. The proposed technique consists of three main stages: 1) spectral unmixing; 2) the SRM algorithm; and 3) the self training model (LR^2 to LR). Stages 2 and 3 together comprise the core of the proposed method and stage 1 can be performed independently through any desired technique. The experiments on real HS data verify the low complexity and high performance of the proposed unsupervised SRM technique.

The remainder of this article is organized as follows. Section II, introduces the applied endmember extraction and unmixing techniques. Section III, presents the designed SRM algorithm. In section IV, the proposed self-training model is described. The experiments and discussion on the obtained results are provided in section V. Finally, we conclude with some remarks in section VI.

II. SPECTRAL UNMIXING

A. Endmember Extraction

Some of the best known unsupervised/supervised algorithms for endmember extraction of HS images include N-FINDR, pixel purity index (PPI), manual endmember selection tool (MEST), convex cone analysis (CCA), iterative error analysis (IEA), optical real-time adaptative spectral identification system (ORASIS), simulated annealing algorithm (SAA), and automated morphological endmember extraction (AMEE) [7]. In this paper the PPI algorithm is used [8].

The PPI algorithm consists of three steps. The first step, a "noise-whitening" and dimensionality reduction, is performed by using the minimum noise fraction (MNF) transform [8]. Then, all the points in the resultant N-dimensional MNF-transformed space are projected onto many randomly generated lines (we set the iteration number to 10000) and the points falling at the extremes of each line are counted. The pixels that fall above a desired threshold (set to 2.5) are the purest pixels. These potential endmember pixel spectra are loaded into an interactive N-dimensional visualization tool to be rotated in real time until the desired number of endmembers are visually identified. The extracted endmembers are used for spectral mixture analysis of the HS image.

B. Spectral Mixture Analysis

Despite the higher accuracy of an intimate mixture model, a frequent assumption in HS remote sensing is that the spectral signatures of mixed pixels result from linear combinations of endmember spectra [9], [10]. Furthermore, it has been shown that the intimate model could be linearized to simplify analysis [11]. Accordingly, only linear spectral unmixing is considered in this letter.

In M-dimensional space of endmember spectra, each vector component of an unknown spectra $\mathbf{u} = (u_1, u_2, ..., u_M)$ is composed of a linear combination of endmember spectra. $\mathbf{u}$ is related to

Manuscript received December 26, 2009. This work was supported by the Natural Science Foundation of China under the grants 60972143 and 60972144, and research fund for the doctorial program of higher education of China under the grant 20092302110033.

The authors are with the Department of Information Engineering, School of Electronics and Information Technology, Harbin Institute of Technology, Harbin, Heilongjiang, 150001, China (e-mail: fmianji@ieee.org).

endmembers by the estimation vector $r = (r_1, r_2, ..., r_L)$ with following constraints:

$$\sum_{l=1}^{L} r_l = 1 \text{ and } \quad 0 \le r_l \le 1 \tag{1}$$

where $l \in [1, ..., L]$ and L is the number of endmembers. For a mixture like **u**, the spectral response at wavelength λ_m, $S^u_{\lambda_m}$, is

$$S^u_{\lambda_m} = \sum\nolimits_l r_l S^l_{\lambda_m} \tag{2}$$

where $m \in [1, ..., M]$. The difference between the calculated and actual spectral responses of **u** at λ_m is

$$e_m = (u_m - \sum\nolimits_l r_l S^l_{\lambda_m}). \tag{3}$$

Some algorithms have been developed to minimize the error e_m in a linear mixture model (LMM) according to both the nonnegativity and sum-to-one constraints described by (1). Among them, fully constrained least squares (FCLS) algorithm can efficiently meet both of the constraints and is optimal in terms of least squares error [12]. An FCLS unmixing algorithm is adopted in this work to unmix the HS image according to the LMM.

III. SUPERRESOLUTION MAPPING ALGORITHM

A. Spatial Correlation Model

To define the location of landcover classes within a pixel, an SRM algorithm is adopted. The basis for the proposed SRM technique is the spatial correlation model. Fig. 1(a) shows a fractional window of endmember A obtained through linear spectral unmixing of an HS image. Fig. 1(b) shows a random endmember distribution pattern in the subpixel level, whereas Fig. 1(c) depicts a mapping according to the spatial dependence maximization which is the basis for the proposed spatial correlation model. Nevertheless this is only an example, it simply describes the premise for the utilized model.

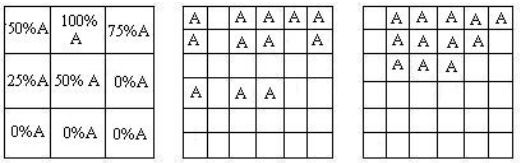

Fig. 1. The basis for the proposed SRM technique.

The mathematical expression of the proposed SRM algorithm is given in (4). $f^l_{i,j}$ is a pixel of the *l*th original LR fractional image and $f(k)^l_{i,j}$ (k=1,2,3,4) are the extracted subpixels for $f^l_{i,j}$.

$$\begin{bmatrix} f^l_{i-1,j-1} & f^l_{i-1,j} & f^l_{i-1,j+1} \\ f^l_{i,j-1} & f^l_{i,j} & f^l_{i,j+1} \\ f^l_{i+1,j-1} & f^l_{i+1,j} & f^l_{i+1,j+1} \end{bmatrix} \rightarrow SRM(f^l_{i,j}) \rightarrow \begin{bmatrix} f(1)^l_{i,j} & f(2)^l_{i,j} \\ f(3)^l_{i,j} & f(4)^l_{i,j} \end{bmatrix} \tag{4}$$

where

$$SRM(f^l_{i,j}) = \underset{k=1,2,3,4}{f(k)^l_{i,j}} = \begin{cases} 1, \text{ if the subpixel of } f_{i,j} \text{ is assigned to target class} \\ 0, \text{ otherwise} \end{cases}.$$

This model utilizes the heuristic tendency of spatially proximate observations to be more alike than distant ones [3], [4], [13]. The necessary spatial distribution rule can be extracted through appropriate learning-based networks. To this end, based on the SRM model in (4), we define the sum of square error (SSE) *E* as follows:

$$E = \frac{1}{2} \sum \left\| \mathbf{T}_z - \mathbf{O}_z \right\|^2 \tag{5}$$

where $\mathbf{T}_z$ is the target output pattern vector denoted by $t(k)^l_{i,j} k = (1,2,3,4)$ and $\mathbf{O}_z$ is the output pattern vector of the network denoted by $f(k)^l_{i,j} k = (1,2,3,4)$. To minimize *E* and obtain the optimal SRM, an effective learning algorithm consisting of a backpropagation neural network (BPNN) is adopted.

B. Adapting the Neural Network

BPNN is one of the most widely used techniques in resolution enhancement [4]. The learning algorithm focuses on determining the connection weights between the nodes of neighbor layers. BPNN has one or more hidden layers of nonlinear neurons followed by an output layer of linear neurons. It is shown that one hidden layer is generally sufficient even for complex cases provided that enough nodes are available [14]. In a 3 layer BPNN (with only one hidden layer) the functions for the output layer nodes are as follows.

$$o_k = g(\sum_{j=1}^{h} w_{jk} y_j - bo_k), \quad k = 1, ..., z \tag{6}$$

where y_j (j=1,2,…,h) are outputs from the hidden layer nodes and o_k (k=1,2,…,z) are outputs from the output layer nodes. v_{ij} (i=1,2,…,n) and w_{jk} are the connection weights between the nodes of layers and bo_k are the bias values for the output layers. All neurons are fully connected and $g(\cdot)$ is the nonlinear activation function, commonly defined as the unipolar sigmoid function

$$g(x) = \frac{1}{1 + e^{-x}}. \tag{7}$$

To overcome the slow convergence and vulnerability to local minima problems in the standard BPNN, a backpropagation learning algorithm with a Fletcher-Reeves version of conjugate gradient is adopted here. The general iterative algorithm of the adapted BPNN for updating the weights and bias values is

$$x_{i+1} = x_i - \alpha_i G_i \tag{8}$$

where x_i is the vector of current weights and biases, G_i is the current gradient, and α_i is the learning rate. The iteration in training stage is repeated until either the error criteria (*E*) or the iteration number (*S*) is satisfied.

The number of the neurons in the input and output layers of the network are constrained by the problem. For the SRM algorithm according to (4) and with a zoom factor of 2 (zf=2), considering the center pixel and its 8 neighbors as the input, the number of neurons in the input and output layers would be 9 and 4, respectively. With the number of hidden layers set to one [14], and considering *E* (SSE) in the training process as the evaluation rule, necessary experiments were carried out to estimate the optimum parameter values of the network. We set the conditions for stopping the training process, i.e., the expected *E* and max iteration number (epochs), to 10^{-3} and 400, respectively. Resultantly, the optimum number of neurons in the hidden layer is set to 25 and the learning rate is set to 0.1. The number of endmembers or mixed pixels in the scene is of negligible importance in defining the optimum parameters.

IV. SELF-TRAINING MODEL

The key idea of this article is training of the designed SRM algorithm with the $LR^2 \rightarrow LR$ mapping model. In other words, the LR image, which is supposed to be enhanced, is also used for the training of the SRM algorithm. The complete processing scheme is depicted in Fig. 2. It mainly includes a soft classification through spectral unmixing (to exploit the spectral information of the LR image) followed by a spatial resolution enhancement process on the obtained fractional images. In this sequence, the later stage integrates the spatial information of the LR image with its spectral information exploited in the former stage.

After endmember extraction, using the PPI method, the linear spectral unmixing is applied to the LR HS image with the help of the LMM and FCLS algorithm to obtain the LR fractional images $f_{x,y}^{l}$ $(l = 1, 2, ..., L)$. These images are then subsampled using a 2×2 mean filter. The corresponding LR^2 fractional images $f_{x,y}^{\prime l}$ are thus obtained. The derived LR^2 and LR fractional images are used for training of the designed SRM algorithm as follows.

1) Using a 3×3 window centered at every pixel of each $f_{x,y}^{\prime l}$ (Fig. 1(a)), with the exception of the pixels of the first and last rows and columns, the input vector is constructed using the batch approach.
2) The target vector is constructed by combining the corresponding pixels from each $f_{x,y}^{l}$, however, with a 2×2 window (the four subpixels at the middle of Fig. 1(c)).
3) The input and target vectors are used to train the SRM algorithm (using BPNN) according to the spatial correlation model.

Finally, the trained SRM algorithm is applied to the LR fractional images ($f_{x,y}^{l}$) and the spatial relation between the endmember abundances in each pixel and the neighboring pixels is exploited. As is shown in Fig. 2, there is no need for any HR sample or other secondary source of data in our approach.

V. EXPERIMENTS AND RESULTS

In the experiments discussed in this section, except the last experiment, we consider the original image as the HR image. The original image can therefore be retrieved from its subsampled version (LR) using the proposed unsupervised SRM algorithm. To benchmark the proposed unsupervised SRM algorithm, it is quantitatively compared with the following two approaches:

1) *The supervised version of the same technique:* We applied the proposed method in supervised fashion for comparison [15]. This approach uses the same SRM algorithm. The only difference is that some HR samples and the corresponding LR samples are used to construct the target and input vectors for the training purpose.

2) *A very efficient unsupervised SRM method proposed by Tatem et al. (2001):* It utilizes Hopfield neural network (HNN) to enhance the same LR fractional images (outputs of the unmixing process) [3]-[5]. The HNN-based method converts the subpixel mapping task into a minimum optimization model, where the spatial dependence is modeled as an energy function. A "best guess" map of the spatial distribution of the class components in each pixel is obtained through minimization of the energy function. Necessary experiments are carried out on different samples to estimate the optimum parameters for the developed HNN program with zf=2. The size of the input window to the energy function and the iteration number are set to 3×3 (center pixel and its 8 neighbors) and 3000, respectively.

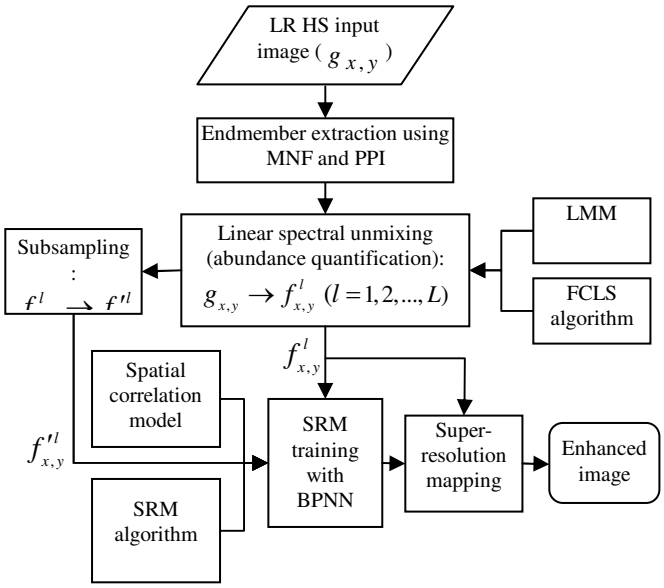

Fig. 2. Outline of the proposed self-training SRM algorithm

A. Data

The following two data sets were chosen for our experiments: the ground truth map (Dataset-I) of Indian Pines data, and the San Diego image (Dataset-II) collected by the Airborne Visible/Infrared Imaging Spectrometer (AVIRIS). Dataset-I, a 144×144 image shown in Fig. 3(a), is used to verify the performance of the proposed SRM technique on real world landcover patterns without the possible influence of the endmember extraction and unmixing process. We applied the proposed SRM algorithm to the individual landcovers of Dataset-I, assuming they are the fractional images of Indian Pines data. It is worth noting that each of the landcover classes of Indian Pines data are dominated by highly mixed pixels resulting from the early growth cycle of agricultural features. Therefore, our binary assumption in class fraction abundances is not fully realistic for this data set. Indeed, applying the proposed SRM algorithm to the real fractional images of Indian Pine data leads to different results.

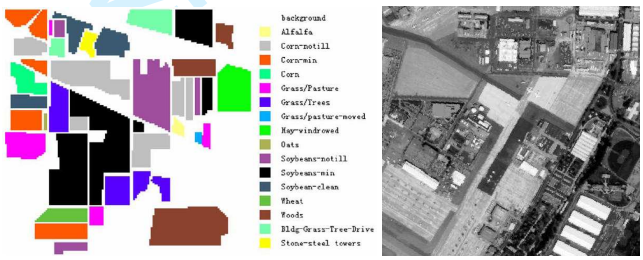

(a) (b)

Fig. 3. (a) The hard classification map of Indian Pines data (Dataset-I). (b) A single spectral channel of Dataset-II.

After removal of the water absorption regions, low SNR and bad bands from Dataset II, 126 available bands from the original data remained in the 0.4–1.8 μm wavelength range. A single spectral channel (wavelength = 0.5277 μm) of the original Dataset-II is shown in Fig. 3(b). Experiments on Dataset-II measured the performance of the algorithm in whole.

B. Experiment on Dataset-I

In this experiment, we used the following eight landcovers from Dataset-I as the original (HR) fractional images: soybeans-min, soybean-clean, woods, grass/trees, soybeans-notill, grass/pasture, alfalfa, and grass/pasture/moved. These HR fractional images were

subsampled with 2×2 and 4×4 mean filters to get the corresponding LR and LR^2 fractional images. To construct the input vector, we used all the nonzero pixels from the LR^2 fractional images (except the pixels from the first and last rows and columns), and some zero pixels from the soybean-min's LR^2 fractional images. Using only nonzero pixels from seven of the LR^2 fractional images is due to the fact that they all consist of considerable empty areas. In total, 625 pixels from the LR^2 fractional images were used to construct the input vector based on the methodology described in section IV.

The target vector was constructed by combining four corresponding pixels from the LR fractional images for each of these designated pixels. The input and target vectors were used for training the SRM algorithm. The trained SRM was then applied to all the selected LR fractional images to enhance them. The subsampled, enhanced, and original HR images for two of the landcovers, namely, Soybean-min and Soybean-clean are shown in Fig. 4 for visual evaluation.

As a reference for quantitative comparison, the proposed unsupervised technique was compared with its supervised version and also with the HNN technique in terms of root mean square error (RMSE) and correlation coefficient (CC). To train the supervised version, we utilized the other landcovers of Dataset-I, i.e., corn-notill, corn-min, corn, oats, and wheat, in the original form as the HR samples. These HR samples were subsampled for constructing the input vector and were used in the original form to construct the target vector. The obtained results verify the good performance of the proposed unsupervised method for all the landcovers. Tables I and II show the related RMSE and CC for the proposed and benchmarking techniques for four of the landcovers.

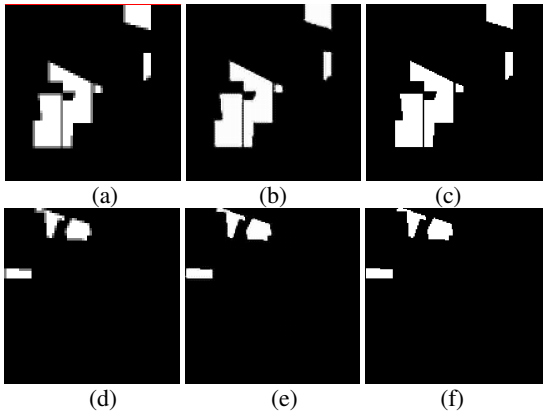

(a) (b) (c) (d) (e) (f)

Fig. 4. Experimental results on Dataset-I. (a), (b), and (c) the subsampled, enhanced and original image for soybean-min, respectively. (d), (e), and (f) the subsampled, enhanced, and original image for soybean-clean, respectively.

TABLE I
RMSE VALUES FOR DIFFERENT TECHNIQUES WITH DATASET-I

	Soybean-min	Soybean-clean	Woods	Grass/ Trees
Proposed-unS	0.0371	0.0264	0.0214	0.0321
Proposed-S	0.0399	0.0216	0.0202	0.0275
HNN	0.0491	0.0271	0.0381	0.0457

TABLE II
CC VALUES FOR DIFFERENT TECHNIQUES WITH DATASET-I

	Soybean-min	Soybean-clean	Woods	Grass/ Trees
Proposed-unS	0.9937	0.9886	0.9964	0.9860
Proposed-S	0.9927	0.9923	0.9968	0.9897
HNN	0.9689	0.9935	0.9941	0.9804

C. Experiments on Dataset-II

Experiment on LR Dataset-II: A region of interest (ROI1) of the original Dataset-II is shown in Fig. 5(a) as the HR image. All necessary bands of HR ROI1 were first subsampled with the 2×2 mean filter. Then, the obtained LR ROI1 (Fig. 5(b)) was processed by the PPI algorithm and linear spectral unmixing program. The extracted LR ROI1 fractional images corresponded to four endmembers: concrete, airplane, asphalt, and sand. These images were then subsampled again with the 2×2 mean filter to provide the necessary LR^2 ROI1 fractional images. We made the input and target vectors, using these LR^2 and LR fractional images, according to the method described in section IV. After training of the SRM algorithm, we applied it to the LR ROI1 fractional images to obtain the spatially enhanced results (Fig. 6).

For the supervised version of the proposed technique, another region of Dataset-II, ROI2 (Fig. 5(c)), was used in original resolution as the HR sample set. Therefore, we trained the SRM algorithm with the LR fractional images derived from ROI2 with known HR information. To this end, all necessary bands of ROI2 were first subsampled with the 2×2 mean filter to obtain LR ROI2. After unmixing of both ROI2 and LR ROI2, the input and target vectors were constructed using the obtained fractional images according to the method described in section IV. The SRM algorithm was finally trained and applied to the LR ROI1 fractional images for resolution enhancement.

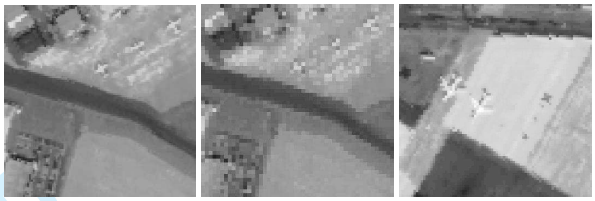

(a) (b) (c)

Fig. 5. Dataset-II. (a) and (b) original and subsampled ROI1. (c) original ROI2.

The RMSE and CC of the enhanced images obtained through both versions of the proposed method are compared with the results of the HNN technique in Tables III and IV. As is shown, the performance of the proposed technique is comparable with the two other techniques. The most important criteria is that the computation time for the SRM part of the proposed technique is only few seconds (12s for training and 1.5s for test) whereas it is more than 30 minutes for the HNN technique in a common computing environment. It is worth mentioning that the endmember extraction and unmixing process for all the experiments are the same. The proposed self-training technique has a big advantage over the HNN technique for real-time systems.

Experiment on original Dataset-II: In this experiment we evaluated the performance of the proposed unsupervised method for resolution enhancement of the original ROI1, i.e., the original ROI1 was considered the LR (not HR) image. To this end, the fractional images derived from the original ROI1 (Fig. 5(a)) and the subsampled ROI1 (Fig. 5(b)) were used as the LR and LR^2 images, respectively. Then, the input and target vectors were constructed according to section IV. The SRM algorithm was subsequently trained and finally applied on the LR ROI1 fractional images. The enhanced resolution results for three of the landcovers are depicted in Fig. 7. A visual evaluation of the results and comparison with the corresponding original images in Figs. 6 (c), (f), and (l), qualitatively verifies the effectiveness of the proposed method. The obtained

results present a higher definition for the small targets as well as sharper edges for the landcovers.

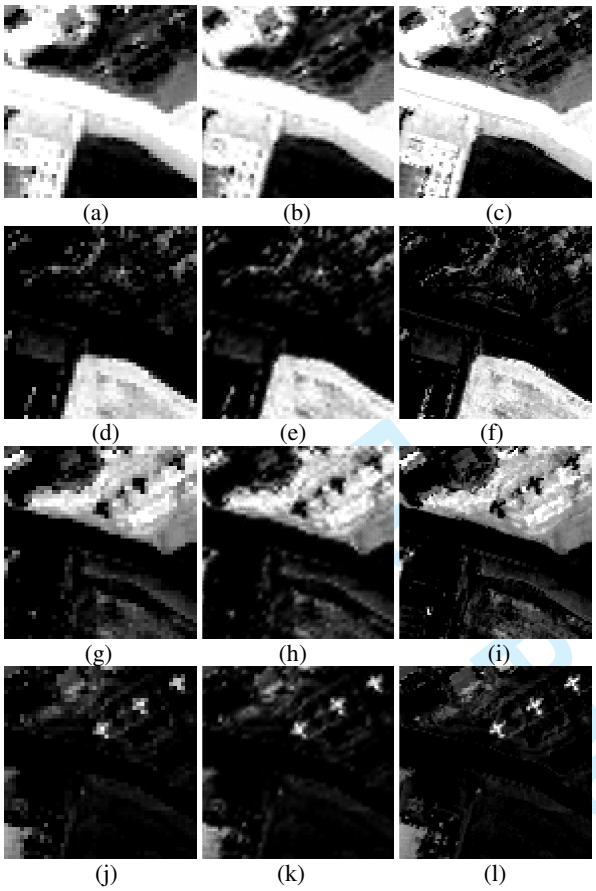

Fig. 6. Experimental results on Dataset-II. (a), (d), (g), and (j) the LR images for asphalt, sand, concrete, and airplane, respectively. (b), (e), (h), and (k) the resolution enhanced images for asphalt, sand, concrete, and airplane, respectively. (c), (f), (i), and (l) the original HR images for asphalt, sand, concrete, and airplane, respectively.

TABLE III
RMSE VALUES FOR DIFFERENT TECHNIQUES WITH DATASET-II

	Asphalt	Sand	Concrete	Airplane
Proposed-unS	0.0787	0.0830	0.0695	0.0525
Proposed-S	0.0786	0.0729	0.0861	0.0511
HNN	0.0981	0.0756	0.1034	0.0604

TABLE IV
CC VALUES FOR DIFFERENT TECHNIQUES WITH DATASET-II

	Asphalt	Sand	Concrete	Airplane
Proposed-unS	0.9787	0.9684	0.9562	0.9149
Proposed-S	0.9813	0.9733	0.9650	0.9106
HNN	0.9708	0.9716	0.9529	0.9020

VI. CONCLUSION

A novel self-training resolution enhancement technique for HS imagery through SMA and SRM is proposed in this paper. The known superresolution mapping between the subsampled LR test image (LR^2) and the LR test image is simulated and extrapolated through a learning-based SRM algorithm to build an efficient spatial correlation model. The experiments verify its high performance.

The advantages of the proposed technique are: 1) it is independent of secondary HR source of data or *a priori* information about the test HS image; 2) its resolution is high; and 3) it is very fast. In conclusion, the proposed technique is useful for real-time applications such as target recognition and tracking.

Fig. 7. Experimental results for resolution enhancement of the original Dataset-II. (a), (b), and (c) the enhanced images for asphalt, sand, and airplane, respectively.

REFERENCES

[1] M.T. Eismann and R.C. Hardie, "Hyperspectral resolution enhancement using high-resolution multispectral imagery with arbitrary response functions," *IEEE Trans. Geosci. Remote. Sens.*, vol. 43, no. 3, pp. 455–465, Mar. 2005.

[2] G.M. Foody, "Sharpening fuzzy classification output to refine the representation of sub-pixel landcover distribution," *Int. J. Remote Sens.*, vol. 19, no. 13, pp. 2593–2599, 1998.

[3] M.Q. Nguyen, P.M. Atkinson, and H.G. Lewis, "Superresolution mapping using a Hopfield neural network with fused images," *IEEE Trans. Geosci. Remote Sens.*, vol. 44, no. 3, pp. 736–749, Mar. 2006.

[4] Y. Gu, Y. Zhang, and J. Zhang, "Integration of spatial-spectral information for resolution enhancement in hyperspectral images," *IEEE Trans. Geosci. Remote Sens.*, vol. 46, no. 5, pp. 1347-1358, May 2008.

[5] A.J. Tatem, H.G. Lewis, P.M. Atkinson, and M.S. Nixon, "Superresolution target identification from remotely sensed images using a Hopfield neural network," *IEEE Trans. Geosci. Remote Sens.*, vol. 39, no. 4, pp. 781–796, Apr. 2001.

[6] Y. Ge, S. Li, and V. C. Lakhan, "Development and testing of a subpixel mapping algorithm," *IEEE Trans. Geosci. Remote Sens.*, vol. 47, no. 7, pp. 2155-2164, Jul. 2009.

[7] A. Plaza, P. Martinez, R. Perez, and J. Plaza, "A quantitative and comparative analysis of endmember extraction algorithms from hyperspectral data," *IEEE Trans. Geosci. Remote Sens.*, vol. 42, no. 3, pp. 650-663, Mar. 2004.

[8] J. W. Boardman, F. A. Kruse, and R. O. Green, "Mapping target signatures via partial unmixing of AVIRIS data," in *Summaries of the VI JPL Airborne Earth Science Workshop*. Pasadena, CA, 1995.

[9] J. Bolton and P. Gader, "Random set framework for context-based classification with hyperspectral imagery," *IEEE Trans. Geosci. Remote Sens.*, vol. 47, no. 11, pp. 3810–3821, Nov. 2009.

[10] S. K. Das and R. Singh, "Performance of kriging-based soft classification on wiFS-IRS-1D image using ground hyperspectral signatures," *IEEE Geosci. Remote Sens. Lett.*, vol. 6, no. 3, pp. 453–457, Jul. 2009.

[11] N. Dobigeon, J.Y. Tourneret, and C.I. Chang, "Semi-supervised linear spectral unmixing using a hierarchical Bayesian model for hyperspectral imagery," *IEEE Trans. Signal Process.*, vol. 56, no. 7, pp. 2684-2695, Jul. 2008

[12] D. Heinz and C.I. Chang, "Fully constrained least squares linear spectral mixture analysis method for material quantification in hyperspectral imagery," IEEE *Trans. Geosci. Remote Sens.*, vol. 39, no. 3, pp. 529–545, Mar. 2001.

[13] J. A. Richards and X. Jia, "Using suitable neighbors to augment the training set in hyperspectral maximum likelihood classification," *IEEE Geosci. Remote Sens. Lett.*, vol. 5, no. 4, pp. 774–777, Oct. 2008.

[14] K. Hornik, M. Stinchcombe, and H. White, "Multilayer feedforward networks are universal approximators," *Neural Networks*, vol. 2, no. 5, pp. 359–366, 1989.

[15] F. A. Mianji, Y. Zhang, Y. Gu, and A. Babakhani, "Spatial-spectral data fusion for resolution enhancement of hyperspectral imagery," in *Proc. IGARSS*, Cape Town, South Africa, Jul. 2009, pp. 1011–1014.